

Superradiance Instabilities of Charged Black Holes in Einstein-Maxwell-scalar Theory

Guangzhou Guo^{a,*}, Peng Wang^{a,†}, Houwen Wu^{a,b,‡} and Haitang Yang^{a,§}

^a*Center for Theoretical Physics, College of Physics,
Sichuan University, Chengdu, 610064, China and*

^b*Department of Applied Mathematics and Theoretical Physics,
University of Cambridge, Wilberforce Road, Cambridge, CB3 0WA, UK*

We study time evolutions of charged scalar perturbations on the background of a charged hairy black hole, in which the perturbations can be governed by a double-peak effective potential. By extracting quasinormal modes from the waveform of scalar perturbations, we discover that some quasinormal modes, which are trapped in a potential well between two potential peaks, can be superradiantly amplified. These superradiant modes make the hairy black hole unstable against charged scalar perturbations. Moreover, it is found that the superradiant modes arise from the competition between the superradiant amplification caused by tunneling through the outer potential barrier and the leakage of modes through the inner potential barrier into the black hole.

arXiv:2301.06483v1 [gr-qc] 16 Jan 2023

* gzguo@stu.scu.edu.cn

† pengw@scu.edu.cn

‡ hw598@damtp.cam.ac.uk

§ hyanga@scu.edu.cn

CONTENTS

I. Introduction	2
II. Superradiance on Hairy Black Hole Spacetime	5
A. Black Hole Solution	5
B. Superradiance of a Charged Scalar Field	6
III. Superradiant Instabilities of Hairy Black Holes	10
A. Single-peak Potential	11
B. Potential with Two Well-separated Peaks	12
C. Potential with Two Adjacent Peaks	14
IV. Conclusions	17
Acknowledgments	18
References	18

I. INTRODUCTION

With the advent of successful detections of gravitational waves by LIGO and Virgo, black hole spectral analysis makes us accessible to test general relativity in the strong field regime [1]. In particular, the ringdown stage of binary black hole mergers can be precisely modeled by a superposition of quasinormal modes of remnant black holes [2]. Therefore, extracting quasinormal modes from gravitational waves provides a promising tool to disclose the parameters of black holes, e.g., the black hole mass, spin and charge [3, 4]. Moreover, quasinormal modes have been shown to encode geometric information of black holes [5–11]. In the eikonal limit, the real part of quasinormal modes corresponds to the angular velocity of null circular geodesics, and the imaginary part to the Lyapunov exponent of the orbits [12]. Additionally, quasinormal modes play a significant role in determining whether the strong cosmic censorship is respected for various black hole models [13–15].

When a black hole spacetime is perturbed, perturbations outside the black hole are usually damped into the event horizon and spatial infinity, leading to a discrete set of quasinormal modes with a negative imaginary part [16–20]. However, the existence of negative energy states can give rise to superradiance, which allows for energy, charge and angular momentum extraction from black

holes [21]. Superradiance phenomenon was discovered when Klein noticed that an beam of electrons can penetrate a step potential without an exponential suppression [22]. Intriguingly, a stationary and axisymmetric spacetime with the presence of an event horizon has been proven to possess the ergoregion, where negative energy states can exist [23]. For a rotating black hole, superradiance is the field-theory version of the Penrose process, in which a test particle can gain energy from the black hole [24]. Analogous to the case of rotating black holes, superradiance phenomenon was also found for charged perturbations around a static and charged black hole [25–27]. Moreover, the second law of black hole thermodynamics implies that waves can extract energy from charged or rotating black holes if the superradiance condition is fulfilled [21, 28].

If extracted energy can pile up outside black holes, superradiance may render the black hole spacetime unstable against small perturbations. Usually, a trapping potential well is needed to accumulate superradiant amplifications of perturbations. On the Kerr background, the effective potential of a massive scalar field can develop a potential well outside the black hole [29]. The outer potential barrier serves as a mirror to reflect scalar waves back to the ergoregion to constantly drain energy from the black hole, resulting in an exponential growth of the scalar field within the potential well. It is expected that superradiant instabilities may make a Kerr black hole evolve into a hairy black hole with boson clouds. Nevertheless, although superradiance can extract up to 29% of the initial black hole mass [24, 30], the low energy-density of boson clouds makes a negligible contribution to the background metric, which indicates that the formation of boson clouds can be well described at a linear level [31]. For a linear perturbation, quasinormal modes with a positive imaginary part were found, which manifests a superradiance instability [32–37].

In Reissner-Nordström (RN) black holes, superradiance instabilities are absent for a massive charged scalar field since conditions for superradiance and the existence of a trapping potential well cannot be simultaneously met [38]. To trigger superradiance instabilities, a mirror-like boundary condition is often imposed for a charged perturbation in the far field to mimic the outer potential barrier of a massive scalar in the Kerr background [39–42]. Notwithstanding, it was found that a potential well of charged scalar perturbations can be formed outside asymptotically-flat charged black holes in scalar-tensor Horndeski theory [43]. Nonetheless, the authors made no attempt to search for superradiant modes. Moreover, unstable superradiant modes were obtained in a charged regular black hole in [44]. However, the origin of these modes, i.e., the existence of a trapping potential well, was not fully discussed.

Recently, a novel class of hairy black holes have been constructed in Einstein-Maxwell-scalar theory to understand the formation of hairy black holes [45]. In particular, the scalar field non-

minimally coupled to the electromagnetic field can trigger the onset of tachyonic instabilities near the event horizon of RN black holes, inducing scalarized RN black holes with secondary scalar hair. Further studies on the Einstein-Maxwell-scalar model have been successively reported in the literature, e.g., different non-minimal coupling functions [46–48], massive and self-interacting scalar fields [49, 50], horizonless reflecting stars [51], stability analysis of hairy black holes [52–56], higher dimensional scalar-tensor models [57], quasinormal modes of hairy black holes [58, 59], two U(1) fields [60], quasitopological electromagnetism [61], topology and spacetime structure influences [62], and hairy black hole solutions in the dS/AdS spacetime [63–66].

Remarkably, we found that scalarized RN black holes can possess two photon spheres outside the event horizon in certain parameter regions [67]. Subsequently, optical appearances of accretion disks, luminous celestial spheres and infalling stars in the scalarized RN black hole background were investigated, showing that an extra photon sphere can lead to bright rings of different radii and noticeably increasing the flux of observed accretion disk images [67, 68], triple higher-order images of a luminous celestial sphere [69], and produce one more cascade of flashes of an infalling star [70]. It is noteworthy that the existence of two photon spheres outside the event horizon of asymptotically-flat black holes has also been reported for dyonic black holes with a quasitopological electromagnetic term and black holes in massive gravity [71–73]. For more details of black holes with multiple photon spheres, one can refer to [74].

More interestingly, the effective potential of a test neutral scalar field around the hairy black holes with double photon spheres has been shown to possess a double-peak profile, which gives rise to long-lived modes trapped in a potential valley [75]. In addition, these long-lived modes are closely related to echo signals observed in black holes with double photon spheres [76]. Motivated by the presence of a potential well for a neutral scalar field, it is natural to explore the existence of a trapping potential well for a charged scalar field and check superradiance instabilities against charged scalar perturbations in the hairy black holes.

The rest of the paper is organized as follows. In section II, after scalarized RN black holes are briefly reviewed, we discuss superradiance for a charged scalar field in the hairy black hole background. Superradiance instabilities and superradiant quasinormal modes of the hairy black holes are studied in section III. We finally summarize our results in section IV. In this paper, we set $16\pi G = 1$ hereafter.

II. SUPERRADIANCE ON HAIRY BLACK HOLE SPACETIME

In this section, we study superradiance of a charged scalar field in static spherically symmetric charged black holes in an Einstein-Maxwell-scalar model and show that such fields can extract energy from the black holes.

A. Black Hole Solution

In the Einstein-Maxwell-scalar model, a scalar field ϕ is minimally coupled to the metric field and non-minimally coupled to the electromagnetic field A_μ , which is described by the action [45],

$$S = \int d^4x \sqrt{-g} \left[\mathcal{R} - 2\partial_\mu \phi \partial^\mu \phi - e^{\alpha\phi^2} F_{\mu\nu} F^{\mu\nu} \right], \quad (1)$$

where \mathcal{R} is the Ricci scalar, $e^{\alpha\phi^2}$ is the coupling function, and $F_{\mu\nu} = \partial_\mu A_\nu - \partial_\nu A_\mu$ is the electromagnetic field strength tensor. For a static and spherically symmetric black hole solution,

$$ds^2 = -N(r)e^{-2\delta(r)} dt^2 + \frac{1}{N(r)} dr^2 + r^2 (d\theta^2 + \sin^2 \theta d\varphi^2),$$

$$A_\mu dx^\mu = \Phi(r) dt \text{ and } \phi = \phi(r), \quad (2)$$

one can obtain the corresponding equations of motion,

$$N'(r) = \frac{1 - N(r)}{r} - \frac{Q^2}{r^3 e^{\alpha\phi^2(r)}} - rN(r) [\phi'(r)]^2,$$

$$[r^2 N(r) \phi'(r)]' = -\frac{\alpha Q^2 \phi(r)}{r^2 e^{\alpha\phi^2(r)}} - r^3 N(r) [\phi'(r)]^3,$$

$$\delta'(r) = -r [\phi'(r)]^2, \quad (3)$$

$$\Phi'(r) = \frac{Q}{r^2 e^{\alpha\phi^2(r)}} e^{-\delta(r)},$$

where the integration constant Q denotes the black hole electric charge, and primes represent derivatives with respect to r .

To solve for the black hole solution from eqn. (3), appropriate boundary conditions should be taken into account. At the event horizon r_h , we impose that

$$N(r_h) = 0, \delta(r_h) = \delta_0, \phi(r_h) = \phi_0, V(r_h) = \Phi_0, \quad (4)$$

where Φ_0 is the electrostatic potential, and δ_0 and ϕ_0 are used to characterize a specific black hole solution. In particular, $\phi_0 = \delta_0 = 0$ corresponds to a scalar-free black hole solution with $\phi = 0$, i.e., a RN black hole. Nevertheless, when nonzero values of ϕ_0 and δ_0 are adopted, a hairy black

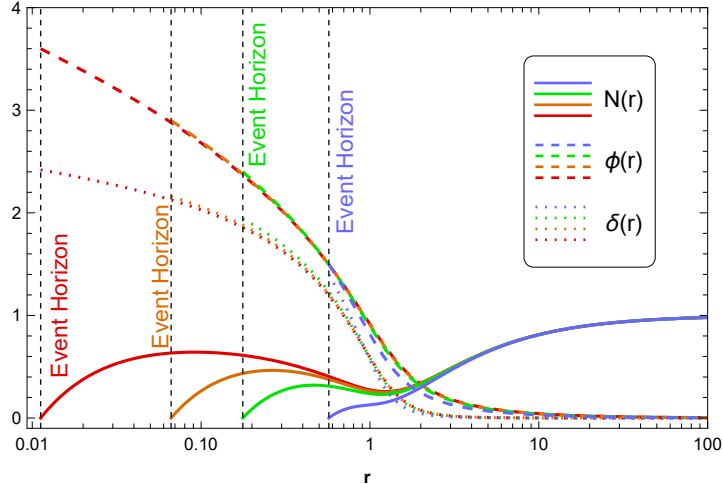


FIG. 1. Hairy black hole solutions with $\alpha = 0.88$ for $Q = 1.0365$ (blue lines), $Q = 1.0629$ (green lines), $Q = 1.0691$ (orange lines) and $Q = 1.0717$ (red lines). The area of the event horizon shrinks as the black hole charge increases.

hole solution with a non-trivial scalar field ϕ can be obtained. At spatial infinity, the black hole solution has the asymptotic expansions,

$$N(r) = 1 - \frac{2M}{r} + \frac{Q^2 + Q_s^2}{r^2} + \dots, \quad \delta(r) = \frac{Q_s^2}{2r^2} + \dots, \quad \phi(r) = \frac{Q_s}{r} + \dots, \quad \Phi(r) = -\frac{Q}{r} + \dots, \quad (5)$$

where M is the black hole mass, and Q_s is the scalar charge. In this paper, we use a shooting method built in the *NDSolve* function of *Wolfram* $\text{\textcircled{R}}$ *Mathematica* to find hairy black hole solutions satisfying the boundary conditions (4) and (5). Thanks to the scaling symmetry, we can set $M = 1$ without loss of generality. In FIG. 1, we present the functions $N(r)$, $\delta(r)$ and $\phi(r)$ of the black hole solutions with $\alpha = 0.88$ for various values of Q .

B. Superradiance of a Charged Scalar Field

We now study a massless charged scalar field Ψ of charge q perturbing the hairy black hole spacetime, which is governed by the Klein-Gordon equation,

$$(\nabla_\mu - iqA_\mu)(\nabla^\mu - iqA^\mu)\Psi = 0. \quad (6)$$

Since the background spacetime is spherically symmetric, we decompose the scalar perturbation Ψ in terms of spherical harmonic functions,

$$\Psi = \sum_{lm} \psi_{lm}(t, r) Y_{lm}(\theta, \varphi) / r. \quad (7)$$

The Klein-Gordon equation is therefore reduced to

$$\frac{\partial^2 \psi(t, r)}{\partial t^2} - \frac{\partial^2 \psi(t, r)}{\partial x^2} - 2iq\Phi(r) \frac{\partial \psi(t, r)}{\partial t} - [q^2 \Phi^2(r) - V(r)] \psi(t, r) = 0, \quad (8)$$

where the indices l and m are suppressed for simplicity, the tortoise coordinate x is defined as $dx/dr = e^{\delta(r)}/N(r)$, and the scalar potential is defined as

$$V(r) = \frac{N(r)}{r^2 e^{2\delta(r)}} \left[1 - N(r) - \frac{Q^2}{r^2 e^{\alpha\phi^2(r)}} + l(l+1) \right]. \quad (9)$$

Note that $x = -\infty$ and $+\infty$ correspond to $r = r_h$ and ∞ , respectively. Given an initial scalar perturbation, solving the partial differential equation (8) gives the evolution of the scalar perturbation in the hairy black hole.

Alternatively, one can study superradiance of the scalar field in the frequency domain. By Fourier transforming $\psi(t, r) = \int d\omega e^{-i\omega t} \psi(r)/2\pi$, eqn. (8) can be written in the Schrödinger-like form,

$$\left[-\frac{d^2}{dx^2} + V_{\text{eff}}(\omega, r) \right] \psi(r) = \omega^2 \psi(r), \quad (10)$$

where we define a frequency-dependent effective potential for the scalar perturbation,

$$V_{\text{eff}}(\omega, r) = V(r) - 2q\omega\Phi(r) - q^2\Phi^2(r). \quad (11)$$

It can show that $V_{\text{eff}}(\omega, \infty) = 0$, and $V_{\text{eff}}(\omega, r_h) = \omega^2 - k_h^2$ with $k_h = \omega + q\Phi(r_h)$. Since $V_{\text{eff}}(\omega, r)$ is constant at the boundaries, a solution ψ_1 to eqn. (10) can have the following asymptotic behavior,

$$\begin{aligned} \psi_1(x) &\sim \mathcal{T}_1 e^{-ik_h x} \text{ for } x \rightarrow -\infty \\ \psi_1(x) &\sim \mathcal{I}_1 e^{-i\omega x} + \mathcal{R}_1 e^{+i\omega x} \text{ for } x \rightarrow +\infty, \end{aligned} \quad (12)$$

which describes an incident wave of amplitude \mathcal{I}_1 from spatial infinity scattering off the effective potential to produce a reflected wave of amplitude \mathcal{R}_1 and a transmitted wave of amplitude \mathcal{T}_1 (see FIG. 2). It should be emphasized that when $\omega < -q\Phi(r_h)$, the phase velocity of the transmitted wave is positive, describing a wave moving away from the horizon. Nevertheless, the group velocity of this wave is negative, e.g., $v_g = -d\omega/dk_h = -1$, indicating that any wavepacket consisting of such modes still moves toward the horizon.

As discussed in [26, 38, 44], the Wronskian identity can be applied to deriving a relation between the scattering coefficients. The Wronskian is constructed by two linearly independent solutions f_1 and f_2 to eqn. (10),

$$W = f_1 \frac{df_2}{dx} - f_2 \frac{df_1}{dx}, \quad (13)$$

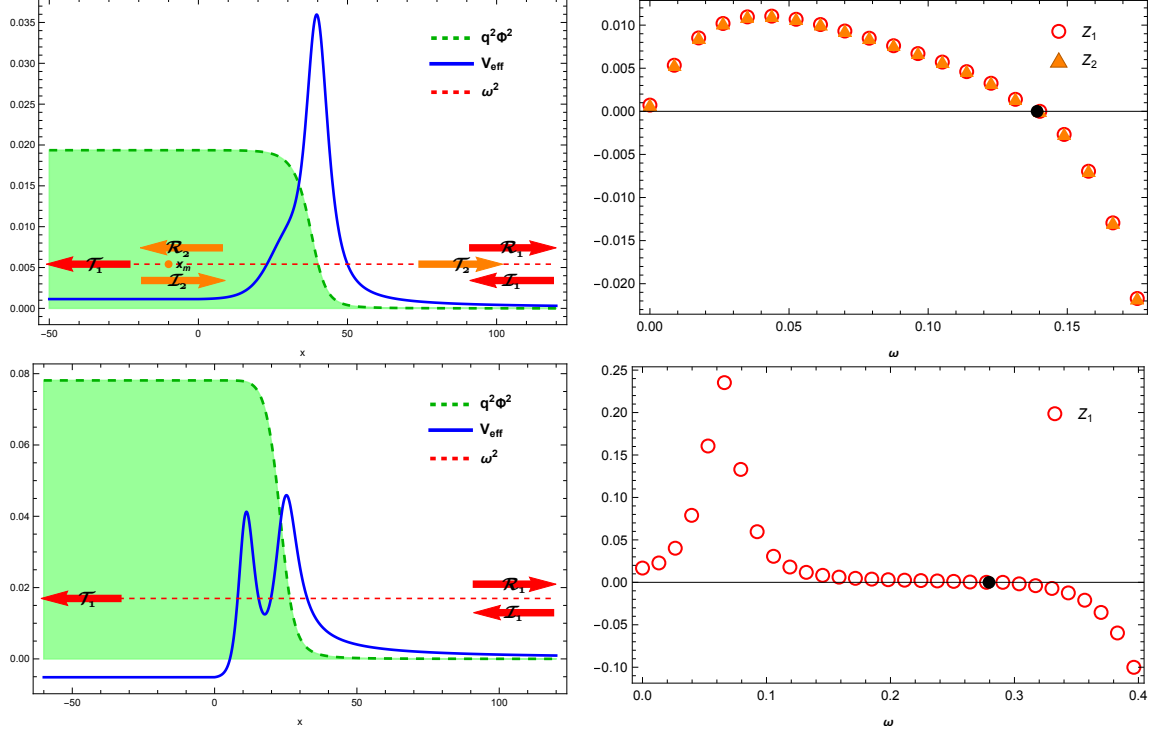


FIG. 2. **Upper Row:** Superradiance of a massless scalar field with $l = 0$ and charge $q = 0.15$ in the hairy black hole with $\alpha = 0.88$ and $Q = 1.0365$. The left panel exhibits the effective potential of the scalar field with $\omega = 0.0736$ and the $q^2\Phi^2$ line bounding a green region, in which the phase and group velocities of the scalar wave are in opposite direction. The existence of the green region can induce superradiance for incident scalar waves travelling in both directions. Amplification factors $Z_1 = \frac{|\mathcal{R}_1|^2}{|\mathcal{I}_1|^2} - 1$ and $Z_2 = \frac{|\mathcal{R}_2|^2}{|\mathcal{I}_2|^2} - 1$ are plotted as a function of the frequency ω in the right panel, which shows that $Z_1 = Z_2$. The superradiance with $Z_1 = Z_2 > 0$ occurs when $\omega < \omega_{\text{up}} \simeq 0.1391$, which is denoted by a black dot. **Lower Row:** Superradiance of a massless scalar field with $l = 0$ and charge $q = 0.3$ in the hairy black hole with $\alpha = 0.88$ and $Q = 1.0629$. The threshold for superradiance with $Z_1 > 0$ to occur is at $\omega = \omega_{\text{up}} \simeq 0.2795$, marked by a black dot. Due to a larger value of qQ , the amplification factor Z_1 significantly increases. The effective potential presents a double-peak structure with a potential well, which provides an arena for superradiance instabilities.

which is independent of the spatial coordinate. Therefore, the Wronskian evaluated at the event horizon equals that evaluated at spatial infinity,

$$|\mathcal{R}_1|^2 - |\mathcal{I}_1|^2 = -\frac{k_h}{\omega} |\mathcal{T}_1|^2, \quad (14)$$

where we set $f_1 = \psi_1$ and $f_2 = \psi_1^*$. It is evident that, when $0 < \omega < -q\Phi(r_h) \equiv \omega_{\text{up}}$, the reflected wave is superradiantly amplified, i.e., $|\mathcal{R}_1| > |\mathcal{I}_1|$. To quantify the superradiance, one can define an amplification factor

$$Z_1 = \frac{|\mathcal{R}_1|^2}{|\mathcal{I}_1|^2} - 1. \quad (15)$$

The amplification factor Z_1 with a given ω can be computed by numerically integrating eqn. (10). The right panels of FIG. 2 display the amplification factor Z_1 as a function of the frequency ω for $l = 0$ waves with different black hole charge Q and scalar field charge q . The black dots denote the superradiance threshold, $Z_1 = 0$, which is found to be consistent with $\omega = \omega_{\text{up}}$. When $\omega < \omega_{\text{up}}$, superradiance is expected to occur, i.e., $Z_1 > 0$. Moreover, it shows that a larger value of qQ would substantially increase the amplification factor of the scalar field. In addition, the corresponding effective potential $V_{\text{eff}}(\omega, x)$ and the function $q^2\Phi^2(x)$ are presented in the left panels of FIG. 2. Interestingly, the lower-left panel shows that there can exist two peaks in the effective potential for a large enough black hole charge. As discussed below, the potential well between the two peaks can temporarily trap scalar perturbations, and hence plays a pivotal role in superradiant instabilities of black holes.

In hairy black holes with a double-peak effective potential, if the scalar field is perturbed between the two potential peaks, an outgoing scalar wave will be incident on the outer potential peak and get scattered. To investigate such case, we consider that an outgoing beam of scalar scatters off a potential barrier, which produces reflected and transmitted waves traveling towards the event horizon and spatial infinity, respectively. As illustrated in the upper-left panel of FIG. 2, this tunneling process is described by a solution ψ_2 to eqn. (10) with the asymptotic behavior,

$$\begin{aligned}\psi_2(x) &\sim \mathcal{I}_2 e^{ik_m x} + \mathcal{R}_2 e^{-ik_m x} \text{ near } x = x_m, \\ \psi_2(x) &\sim \mathcal{T}_2 e^{i\omega x} \text{ for } x \rightarrow +\infty,\end{aligned}\tag{16}$$

where x_m is some reference point, and $k_m = -\sqrt{[\omega + q\Phi(x_m)]^2 - V(x_m)}$ and $\sqrt{[\omega + q\Phi(x_m)]^2 - V(x_m)}$ for $\omega < -q\Phi(x_m)$ and $\omega > -q\Phi(x_m)$, respectively. Since $d\omega/dk_m > 0$, the ingoing reflected wave of amplitude \mathcal{R}_2 and the outgoing incident wave of amplitude \mathcal{I}_2 have negative and positive group velocities, respectively. Evaluating the Wronskian identity for ψ_2 and ψ_2^* at $x = x_m$ and $+\infty$ gives the relation

$$|\mathcal{R}_2|^2 - |\mathcal{I}_2|^2 = -\frac{\omega}{k_m} |\mathcal{T}_2|^2,\tag{17}$$

which shows that the reflected wave has a larger amplitude than that of the incident wave if $0 < \omega < -q\Phi(x_m)$. Similarly, one can define an amplification factor Z_2 ,

$$Z_2 = \frac{|\mathcal{R}_2|^2}{|\mathcal{I}_2|^2} - 1.\tag{18}$$

If x_m is far away from the potential barrier, i.e., $k_m \simeq k_h$, evaluating the Wronskian for the independent solutions ψ_1 and ψ_2 yields

$$k_h \mathcal{I}_1 \mathcal{T}_2 = -\omega \mathcal{I}_2 \mathcal{T}_1.\tag{19}$$

Using eqns. (15), (18) and (19), one can easily infer that $Z_1 = Z_2$.

In the upper-right panel of FIG. 2, we present the amplification factor Z_2 for a charged scalar perturbation with $q = 0.15$ and $l = 0$ in the hairy black hole with $\alpha = 0.88$ and $Q = 1.0365$. As expected, it shows that $Z_2 > 0$ when $0 < \omega < \omega_{\text{up}}$, and $Z_1 = Z_2$. Furthermore, green regions of FIG. 2 are bounded by $q^2\Phi^2(x)$, below which scalar waves have $0 < \omega < -q\Phi(x)$. Our results reveal that superradiance of scalar waves can occur when transmitted waves enter or leave the green regions. Indeed for a scalar mode of frequency ω , one has

$$\omega = -(p_\mu + qA_\mu)\eta^\mu = -p_\mu\eta^\mu - q\Phi, \quad (20)$$

where p_μ is the four momentum, and $\eta^\mu = (\partial/\partial t)^\mu$ is a Killing vector. The local energy of the mode measured by a static observer with four-velocity $u^\mu = N^{-1/2}e^\delta\eta^\mu$ is

$$E = -p_\mu u^\mu = N^{-1/2}e^\delta(\omega + q\Phi), \quad (21)$$

which becomes negative in the green regions. Therefore, if an outgoing scalar wave tunnels through the potential barrier, the transmitted wave leaves the green region and can transport positive energy to spatial infinity, which amplifies negative energy states in the green region. Additionally, when the transmitted part of an incoming scalar wave propagating from spatial infinity enters the green region, negative energy would be carried away to the black hole, and hence the outgoing reflected wave gets superradiantly amplified.

III. SUPERRADIANT INSTABILITIES OF HAIRY BLACK HOLES

As previously mentioned, a particularly important feature of the hairy black hole solution in the Einstein-Maxwell-scalar model is that the presence of a potential well, which are able to trap and amplify a charged scalar field, and hence trigger a superradiant instability. In this section, we investigate the superradiant instability of hairy black holes by computing quasinormal modes of the charged scalar field.

To obtain quasinormal modes, ingoing and outgoing boundary conditions are imposed at the event horizon and spatial infinity,

$$\begin{aligned} \psi &\sim e^{-i[\omega+q\Phi(r_h)]x}, & \text{for } x \rightarrow -\infty, \\ \psi &\sim e^{i\omega x}, & \text{for } x \rightarrow +\infty, \end{aligned} \quad (22)$$

respectively, which selects a discrete set of quasinormal modes of frequency ω_n with the overtone number $n = 0, 1, 2, \dots$. Owing to the boundary conditions (22), the quasinormal frequencies ω are

generically complex, $\omega = \omega^R + i\omega^I$. Especially, a quasinormal mode with $\omega_I > 0$ corresponds to an instability with the instability time scale $1/\omega^I$.

Here, we use time-domain analysis to extract quasinormal frequencies from time evolutions of the scalar field $\psi(t, x)$, which is governed by eqn. (8). Specifically, we employ a finite difference numerical scheme to discretize the partial differential equation (8) [26, 44]. Denoting $\psi_{i,j} = \psi(i\Delta t, j\Delta x)$, $\Phi_j = \Phi(j\Delta x)$ and $V_j = V(j\Delta x)$, the evolution of $\psi(t, x)$ is determined by

$$\psi_{i+1,j} = -\frac{(1 + iq\Phi_j\Delta t)\psi_{i-1,j}}{1 - iq\Phi_j\Delta t} + \frac{\Delta t^2}{\Delta x^2} \frac{\psi_{i,j+1} + \psi_{i,j-1}}{1 - iq\Phi_j\Delta t} + \left[2 - 2\frac{\Delta t^2}{\Delta x^2} - \Delta t^2(V_j - q^2\Phi_j^2)\right] \frac{\psi_{i,j}}{1 - iq\Phi_j\Delta t}, \quad (23)$$

where we set $\Delta t/\Delta x = 1/2$ to avoid numerical divergence in the simulation [26, 77]. Additionally, we assume that the initial condition of $\psi(t, x)$ is a Gaussian wavepacket, $\psi(t=0, x) = \exp\left[-(x-a)^2/2b^2\right]$ and $\psi(t < 0, x) = 0$.

After the late-time waveform of $\psi(t, x)$ is obtained, quasinormal modes can be extracted via the Prony method [2, 26, 44]. In particular, the late-time waveform can be expressed as the superposition of a set of quasinormal modes,

$$\psi(t, x) = \sum_{i=1}^p C_i e^{-i\omega_i(t-t_0)}. \quad (24)$$

For a given integer n , the value of $\psi(t_0 + n\Delta t)$ can be numerically obtained from eqn. (23). By fitting the late-time waveform (24) with $\psi(t_0 + n\Delta t)$ in the time interval between t_0 and $t_0 + N\Delta t$, one can perform the Prony method to obtain the coefficients C_i and the quasinormal frequencies ω_i .

A. Single-peak Potential

We first check superradiant instabilities of hairy black holes against the charged scalar field, whose effective potential has only one maximum. The left panel of FIG. 3 exhibits the time evolution of the scalar field with $q = 0.2$ and $l = 0$ in the hairy black hole with $\alpha = 0.88$ and $Q = 1.0365$. The late-time waveform is an exponential decay, and hence the hairy black hole is stable against the charged scalar perturbation. As anticipated, the imaginary part of the extracted quasinormal mode is negative. The effective potential of the quasinormal mode is presented in the right panel of FIG. 3. Similar to RN black holes, the absence of superradiant instabilities is attributed to the non-existence of a trapping potential well outside the black hole [38].

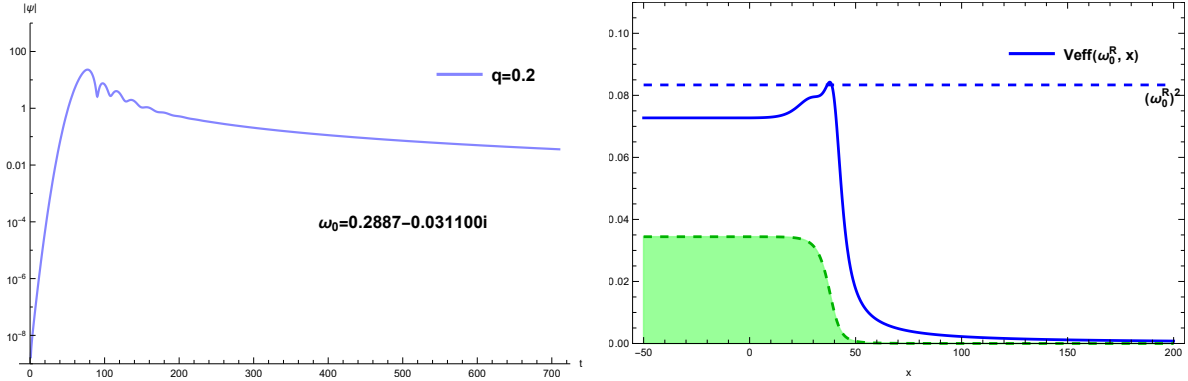


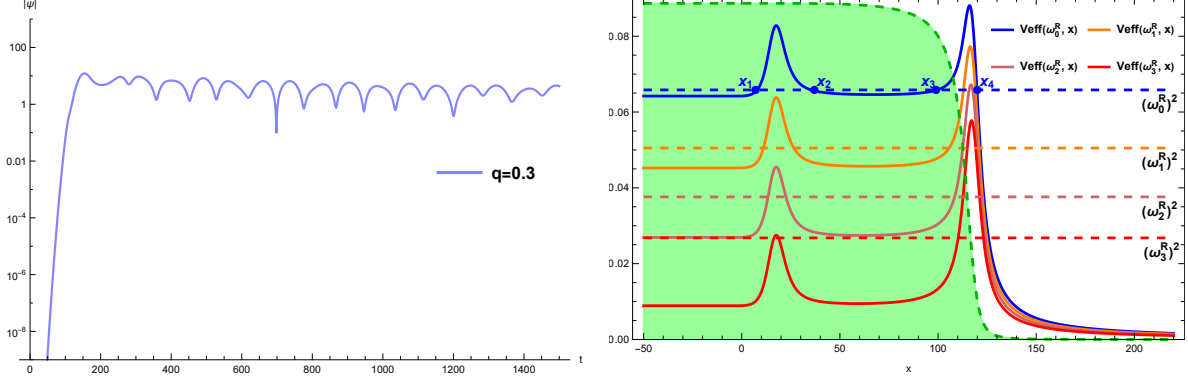
FIG. 3. **Left Panel:** Time evolution of the $q = 0.2$ and $l = 0$ scalar field in the hairy black hole with $\alpha = 0.88$ and $Q = 1.0365$. The observer is located at $x = 114$. At late times, the scalar field decays exponentially, showing that the superradiance instability is absent. The fundamental quasinormal mode ω_0 is extracted from the late-time waveform of the scalar field. **Right Panel:** The effective potential $V_{\text{eff}}(\omega_0^R, x)$ of the fundamental quasinormal mode has only one maximum.

B. Potential with Two Well-separated Peaks

For a large enough black hole charge, there can exist two peaks in the effective potential of the scalar field. Depending on the black hole and field parameters, the separation between the two peaks can be considerably larger than the Compton wavelength of the scalar field, and the potential changes very slowly with x between the two peaks. In this case, WKB approximate solutions of the scalar field can be used in the potential well, which provides insight into superradiance instabilities of hairy black holes.

In FIG. 4, we study the scalar field of $q = 0.3$ and $l = 0$ in the hairy black hole with $\alpha = 0.5$ and $Q = 1.0074$. The upper-left panel shows the time evolution of the scalar field measured at $x = 223$, and the extracted quasinormal modes are presented in the lower table. For each quasinormal mode $\omega_n = \omega_n^R + i\omega_n^I$, the effective potential $V_{\text{eff}}(\omega_n^R, x)$ is displayed in the upper-right panel, which shows that $V_{\text{eff}}(\omega_n^R, x)$ indeed has two well-separated potential peaks. Moreover, the green region in the upper-right panel corresponds to $0 < \omega < -q\Phi(x)$, and scalar waves entering or leaving the green region can be superradiantly amplified.

Intriguingly, the imaginary part of the $n = 0$ mode is positive, indicating that the hairy black hole is unstable against this superradiant mode. To better understand the superradiant mode, we consider a scalar perturbation initially perturbed between the two potential peaks. Afterwards, scalar waves are incident on the two potential barriers, and the transmitted waves carry away the perturbation to the black hole and spatial infinity. As shown in the upper-right panel of FIG. 4, the



Q	q	n	Quasinormal modes	$S_2 - (n + 1/2)\pi$	S_1	S_3	ΔS	Z_{sup}	Z_2
1.0074	0.3	0	$0.2566 + 0.000063i$	+0.353	1.971	1.567	+0.404	-0.029	0.056
		1	$0.2247 - 0.000302i$	+0.185	1.210	1.551	-0.341	-0.202	0.066
		2	$0.1940 - 0.001311i$	+0.027	0.601	1.551	-0.950	-0.838	0.073
		3	$0.1637 - 0.003081i$	-0.024	0.046	1.554	-1.509	-2.834	0.074

FIG. 4. Superradiance instability of the $q = 0.3$ and $l = 0$ scalar field in the hairy black hole with $\alpha = 0.5$ and $Q = 1.0074$. **Upper-Left Panel:** Time evolution of the scalar field measured at $x = 223$. **Upper-Right Panel:** The effective potential $V_{\text{eff}}(\omega_n^R, x)$ of the quasinormal modes has two well-separated peaks. The green region is bounded by $q^2\Phi^2(x)$. **Lower Table:** Quasinormal modes extracted from the time evolution of the scalar field. The $n = 0$ mode is a superradiant mode with $\omega^I > 0$ while the rest modes are damped ones with $\omega^I < 0$. As explained in the main text, $Z_{\text{sup}} + Z_2$ and ΔS can be used to measure the competition between the superradiant accumulation in the potential valley and the leakage of modes through the inner potential barrier. Interestingly, a superradiant/damped mode has positive/negative $Z_{\text{sup}} + Z_2$ and ΔS .

transmitted part of the scalar wave incident on the outer potential barrier leaves the green region, and hence the reflected wave gets superradiantly amplified. The amplification can be characterized by the amplification factor Z_2 , which is defined in eqn. (18). On the other hand, the leakage of the scalar wave through the inner potential barrier can suppress the superradiant amplification. To describe the suppression, one can consider the solution $\psi_{\text{sup}}(x)$,

$$\begin{aligned} \psi_{\text{sup}}(x) &\sim e^{-ik_h x} \text{ for } x \rightarrow -\infty, \\ \psi_{\text{sup}}(x) &\sim \mathcal{I}_{\text{sup}} e^{-ik_m x} + \mathcal{R}_{\text{sup}} e^{+ik_m x} \text{ when } x \text{ is between the two peaks,} \end{aligned} \quad (25)$$

where $\mathcal{I}_{\text{sup}} e^{-ik_m x} / \mathcal{R}_{\text{sup}} e^{+ik_m x}$ represents the ingoing/outgoing mode with a negative/positive group velocity. So one can introduce a suppression factor

$$Z_{\text{sup}} = 1 - \frac{|\mathcal{I}_{\text{sup}}|^2}{|\mathcal{R}_{\text{sup}}|^2}, \quad (26)$$

which is negative if $|\mathcal{R}_{\text{sup}}|^2 < |\mathcal{I}_{\text{sup}}|^2$. Note that more negative Z_{sup} is, the more the leakage through the inner potential barrier suppresses the superradiant amplification. Roughly speaking, the competition between the superradiant amplification and the suppression determines whether trapped modes between the potential peaks can accumulate. In the table of FIG. 4, we list Z_{sup} and Z_2 for each mode and find that the superradiant mode with $\omega^I > 0$ has $Z_{\text{sup}} + Z_2 > 0$ while the damped modes with $\omega^I < 0$ have $Z_{\text{sup}} + Z_2 < 0$.

Alternatively for a quasinormal mode $\omega_n = \omega_n^R + i\omega_n^I$, we define

$$\begin{aligned} S_1 &= \int_{x_1}^{x_2} \sqrt{V_{\text{eff}}(\omega_n^R, x) - (\omega_n^R)^2} dx, \\ S_2 &= \int_{x_2}^{x_3} \sqrt{(\omega_n^R)^2 - V_{\text{eff}}(\omega_n^R, x)} dx, \\ S_3 &= \int_{x_3}^{x_4} \sqrt{V_{\text{eff}}(\omega_n^R, x) - (\omega_n^R)^2} dx, \end{aligned} \quad (27)$$

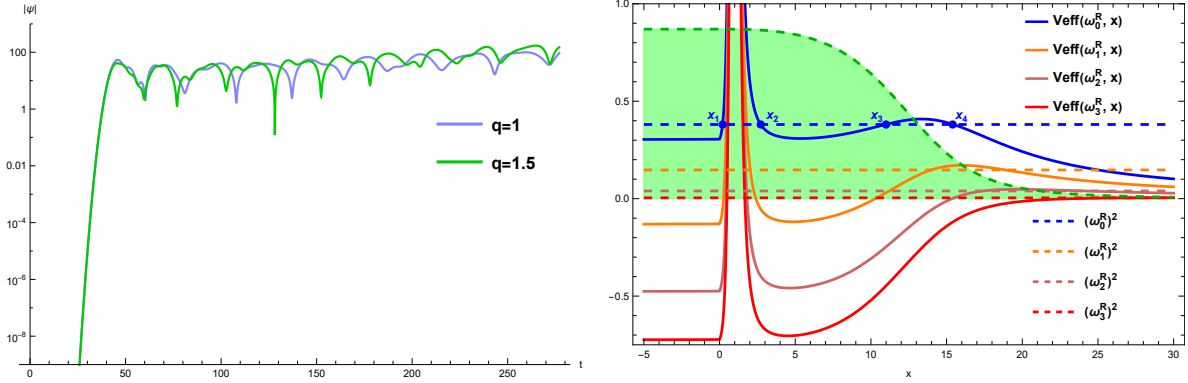
where x_1, x_2, x_3 and x_4 are displayed in the upper-right panel of FIG. 4. As expected, a larger S_1 makes tunneling through the inner potential barrier more difficult and hence reduces the leakage of trapped modes. On the other hand, a larger S_3 makes tunneling through the outer potential barrier more difficult, meaning that less scalar waves with positive energy can escape to spatial infinity. So the superradiance accumulates less trapped modes with negative energy in the potential valley for a larger S_3 . In the table of FIG. 4, S_1, S_3 and $\Delta S \equiv S_1 - S_3$ are presented for each mode. It shows that the sign of ΔS can also be used to reflect which effect wins the competition. Particularly, a positive ΔS implies that the superradiant amplification plays a more dominant role, therefore signaling a superradiant mode. Moreover in the eikonal limit, quasinormal modes trapped in the potential valley were found to satisfy the quantization rule [75],

$$S_2 \approx \left(n + \frac{1}{2}\right) \pi, \quad n = 0, 1, 2, \dots \quad (28)$$

Indeed, the table of FIG. 4 shows that, for each mode, the numerical values of S_2 are well approximated by the WKB result (28).

C. Potential with Two Adjacent Peaks

When the separation between the two potential peaks are not large enough, one cannot obtain Z_{sup} and Z_2 to discuss the amplification and suppression effects. Nevertheless, ΔS can still be employed to describe the competition between the superradiant amplification and the leakage of trapped modes. Roughly speaking, more scalar waves escape to black holes for a smaller S_1 , and



Q	q	n	Quasinormal modes	$S_2 - (n + 1/2)\pi$	S_1	S_3	ΔS
1.0717	1	0	$0.6169 + 0.007770i$	+0.184	2.420	0.580	+1.841
		1	$0.3838 + 0.005220i$	+0.069	2.016	0.583	+1.434
		2	$0.1989 + 0.003615i$	+0.003	1.761	0.461	+1.300
		3	$0.0659 + 0.001938i$	+0.125	1.593	0.189	+1.404
	1.5	0	$1.0541 + 0.010917i$	+0.200	2.362	0.378	+1.983
		1	$0.7939 + 0.007814i$	+0.098	1.935	0.412	+1.524
		2	$0.5749 + 0.005855i$	+0.021	1.646	0.400	+1.246
		3	$0.3868 + 0.004247i$	-0.030	1.420	0.343	+1.077
		4	$0.2293 + 0.002878i$	-0.037	1.240	0.244	+0.996
		5	$0.1081 + 0.001662i$	+0.029	1.107	0.127	+0.979

FIG. 5. **Upper-Left Panel:** Time evolution of the $l = 0$ scalar fields with $q = 1$ and 1.5 in the hairy black hole with $\alpha = 0.88$ and $Q = 1.0717$. The observer is located at $x = 56$. The scalar fields grow at late times, and hence the black hole is unstable against the scalar perturbations. **Upper-Right Panel:** The effective potential $V_{\text{eff}}(\omega_n^R, x)$ of the $q = 1$ scalar field has two adjacent potential peaks. **Lower Table:** All the extracted quasinormal modes are unstable modes and have a positive ΔS .

more scalar perturbations are accumulated in the potential valley for a smaller S_3 . Our results show that, if ΔS is positive, the superradiance effect can compensate the loss of modes leaking into black holes. So trapped modes can accumulate in the potential well, and eventually become superradiantly unstable.

In FIG. 5, we present time evolutions, effective potentials and quasinormal modes of the monopole scalar fields with $q = 1$ and 1.5 in the hairy black hole with $\alpha = 0.88$ and $Q = 1.0717$. Since the $q = 1$ and 1.5 scalar fields have similar effective potentials, we only display the $q = 1$ case in the upper-right panel. Note that the potential valley is mostly in the green region. When scalar waves tunnel through the outer potential barrier and leave the green region, modes trapped

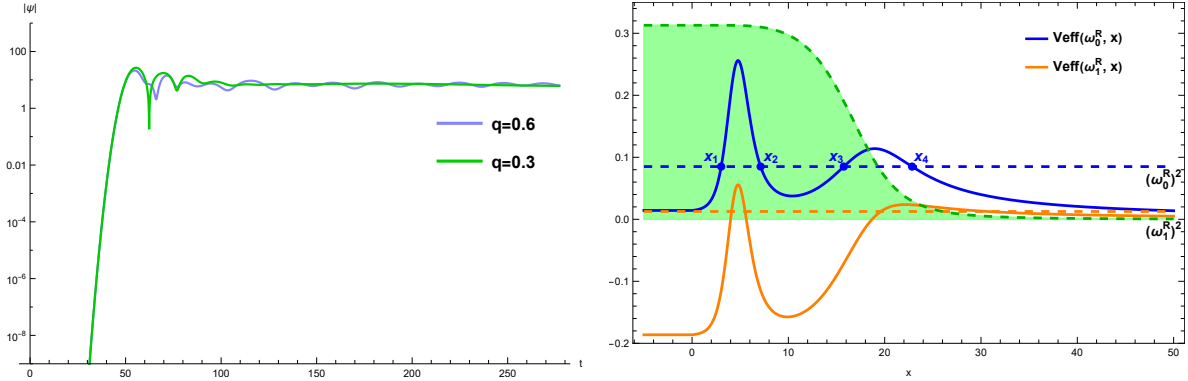
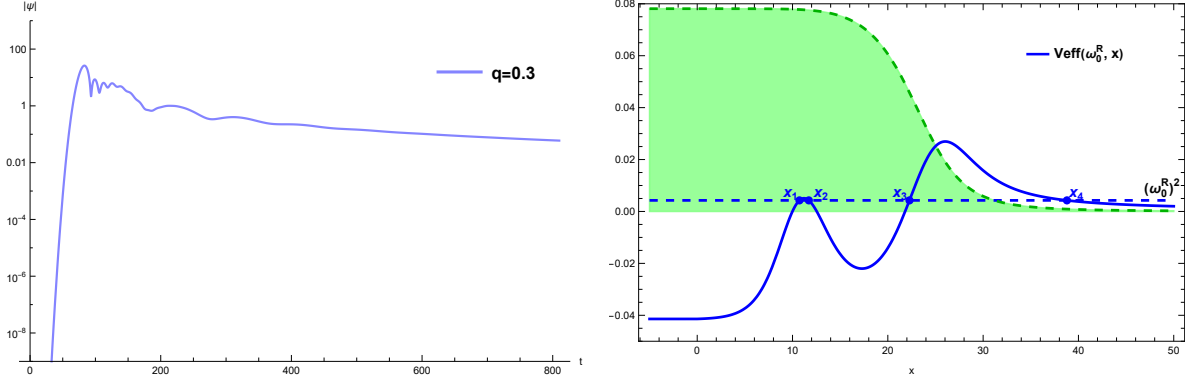


FIG. 6. **Upper-Left Panel:** Time evolution of the $l = 0$ scalar fields with $q = 0.3$ and 0.6 in the hairy black hole with $\alpha = 0.88$ and $Q = 1.0691$. The observer is located at $x = 66$. **Upper-Right Panel:** The effective potential $V_{\text{eff}}(\omega_n^R, x)$ of the $q = 0.6$ scalar field has a potential well. **Lower Table:** The $q = 0.6$ scalar field has one unstable quasinormal mode, which has a positive ΔS .

in the potential valley will get superradiantly amplified. The upper-left panel exhibits that the perturbations grow at late times, indicating an instability of the black hole. The extracted quasinormal modes are listed in the table of FIG. 5, and all these modes are found to be superradiant mode with positive imaginary parts. With a given n , the scalar field with $q = 1.5$ has a larger imaginary part of the quasinormal mode than that with $q = 1$. This observation is expected since superradiant amplifications become stronger at a larger qQ . Moreover, the superradiant modes all have a positive ΔS and approximately satisfy the quantization rule (28).

In FIG. 6, we consider the scalar perturbations with the multipole number $l = 0$ and the charge $q = 0.3$ and 0.6 around the hairy black hole with $\alpha = 0.88$ and $Q = 1.0691$. Only one unstable mode, i.e., ω_0 of the $q = 0.6$ scalar field, is found, and its effective potential is displayed as a blue curve in the upper-right panel. In addition, ΔS of the stable and unstable modes is negative and positive, respectively. FIG. 7 discusses the scalar field with $l = 0$ and $q = 0.3$ in the hairy black hole with $\alpha = 0.88$ and $Q = 1.0629$. Owing to a small S_1 , most of trapped modes can tunnel through the inner barrier and escape to the black hole. Therefore, there is no superradiant mode, and only a stable mode is obtained. Again, this stable mode has a negative ΔS .



Q	q	n	Quasinormal modes	$S_2 - (n + 1/2)\pi$	S_1	S_3	ΔS
1.0629	0.3	0	$0.0653 - 0.016946i$	-0.276	0.022	1.458	-1.436

FIG. 7. Time evolution at $x = 105$, effective potential and quasinormal mode of the $l = 0$ and $q = 0.3$ scalar perturbation in the hairy black hole with $\alpha = 0.88$ and $Q = 1.0629$. Due to a high tunneling rate through the inner potential barrier, only one stable mode is found.

IV. CONCLUSIONS

In this paper, we investigated superradiance and superradiant instabilities of charged scalar perturbations in hairy black hole spacetime, where a real scalar field is minimally coupled to the gravity sector and non-minimally coupled to the electromagnetic field with an exponential coupling function. It showed that a charged scalar wave of frequency ω can be superradiantly amplified when $\omega < -q\Phi(r_h)$. Moreover, we found that the energy of the scalar mode measured by a local observer is negative if $\omega < -q\Phi(r)$. In the figures of this paper, the green regions represent scalar modes with $\omega < -q\Phi(r)$, which are negative energy states. When the transmitted waves enter/leave the green regions, they carry away negative/positive energies to the black hole/spatial infinity. Hence, the reflected waves with positive/negative energy are superradiantly amplified.

To trigger a superradiant instability, two ingredients, i.e., the existence of a trapping potential well and superradiant amplification of trapped modes, are required. Interestingly, we observed that, in certain parameter regimes, the effective potential of the scalar field can develop a potential well between two potential peaks outside the black hole, which can trap some quasinormal modes. If the trapped modes are in the green regions, they are negative energy states in the potential well. The transmitted waves tunneling through the outer potential barrier superradiantly amplify the trapped modes by transporting positive energy to spatial infinity. On the contrary, the transmitted waves tunneling through the inner potential barrier carry away negative energy to

black holes and hence tend to suppress the superradiant amplification. The competition between the two effects would determine whether the trapped modes can grow and destabilize the black hole spacetime. Remarkably, we discovered the existence of superradiant quasinormal modes with a positive imaginary part of the frequency, which renders the black hole spacetime unstable. In addition, it showed that ΔS can be used to describe the competition between the amplification and suppression. Specifically, our results revealed that unstable and stable modes have positive and negative ΔS , respectively.

It should be emphasized that the trapping potential well of a massive scalar field on the Kerr background lies outside the ergoregion, where negative energy states exist [29]. So trapped superradiant modes are positive energy states in the potential well. Increasing the width or height of the inner potential barrier leads to the decrease of the transmitted wave transporting negative energy to the Kerr black hole, which alleviates the superradiant instability. However in the charged hairy black holes, a smaller transmission coefficient through the inner potential barrier favors the accumulation of trapped modes with negative energy, and hence aggravates the superradiant instability.

Finally, it is desirable to explore the possible end state of the hairy black holes under charged perturbations. Beyond the linear analysis in this paper, a full nonlinear analysis is necessary to track evolutions of the background metric, which provides a further understanding on how trapped superradiant modes affect underlying spacetime. Lately, the “trapping instability” induced by stable light rings of ultracompact objects has been confirmed, and two end states of ultracompact bosonic stars have been identified [78, 79]. The fully nonlinear numerical evolutions of hairy black holes suffered from superradiant instabilities may shed light on the fate of stable photon spheres.

ACKNOWLEDGMENTS

We are grateful to Qingyu Gan and Xin Jiang for useful discussions and valuable comments. This work is supported in part by NSFC (Grant No. 12105191, 12275183, 12275184 and 11875196). Houwen Wu is supported by the International Visiting Program for Excellent Young Scholars of Sichuan University.

-
- [1] B.P. Abbott et al. Observation of Gravitational Waves from a Binary Black Hole Merger. *Phys. Rev. Lett.*, 116(6):061102, 2016. [arXiv:1602.03837](https://arxiv.org/abs/1602.03837), [doi:10.1103/PhysRevLett.116.061102](https://doi.org/10.1103/PhysRevLett.116.061102). I
- [2] Emanuele Berti, Vitor Cardoso, Jose A. Gonzalez, and Ulrich Sperhake. Mining information from

- binary black hole mergers: A Comparison of estimation methods for complex exponentials in noise. *Phys. Rev. D*, 75:124017, 2007. [arXiv:gr-qc/0701086](#), [doi:10.1103/PhysRevD.75.124017](#). I, III
- [3] Richard H. Price and Gaurav Khanna. Gravitational wave sources: reflections and echoes. *Class. Quant. Grav.*, 34(22):225005, 2017. [arXiv:1702.04833](#), [doi:10.1088/1361-6382/aa8f29](#). I
- [4] Matthew Giesler, Maximiliano Isi, Mark A. Scheel, and Saul Teukolsky. Black Hole Ringdown: The Importance of Overtones. *Phys. Rev. X*, 9(4):041060, 2019. [arXiv:1903.08284](#), [doi:10.1103/PhysRevX.9.041060](#). I
- [5] Valeria Ferrari and Bahram Mashhoon. New approach to the quasinormal modes of a black hole. *Phys. Rev. D*, 30:295–304, 1984. [doi:10.1103/PhysRevD.30.295](#). I
- [6] Hans-Peter Nollert. TOPICAL REVIEW: Quasinormal modes: the characteristic ‘sound’ of black holes and neutron stars. *Class. Quant. Grav.*, 16:R159–R216, 1999. [doi:10.1088/0264-9381/16/12/201](#).
- [7] Huan Yang, David A. Nichols, Fan Zhang, Aaron Zimmerman, Zhongyang Zhang, and Yanbei Chen. Quasinormal-mode spectrum of Kerr black holes and its geometric interpretation. *Phys. Rev. D*, 86:104006, 2012. [arXiv:1207.4253](#), [doi:10.1103/PhysRevD.86.104006](#).
- [8] R. A. Konoplya and Z. Stuchlík. Are eikonal quasinormal modes linked to the unstable circular null geodesics? *Phys. Lett. B*, 771:597–602, 2017. [arXiv:1705.05928](#), [doi:10.1016/j.physletb.2017.06.015](#).
- [9] Kimet Jusufi. Quasinormal Modes of Black Holes Surrounded by Dark Matter and Their Connection with the Shadow Radius. *Phys. Rev. D*, 101(8):084055, 2020. [arXiv:1912.13320](#), [doi:10.1103/PhysRevD.101.084055](#).
- [10] B. Cuadros-Melgar, R. D. B. Fontana, and Jeferson de Oliveira. Analytical correspondence between shadow radius and black hole quasinormal frequencies. *Phys. Lett. B*, 811:135966, 2020. [arXiv:2005.09761](#), [doi:10.1016/j.physletb.2020.135966](#).
- [11] Wei-Liang Qian, Kai Lin, Xiao-Mei Kuang, Bin Wang, and Rui-Hong Yue. Quasinormal modes in two-photon autocorrelation and the geometric-optics approximation. 9 2021. [arXiv:2109.02844](#). I
- [12] Vitor Cardoso, Alex S. Miranda, Emanuele Berti, Helvi Witek, and Vilson T. Zanchin. Geodesic stability, Lyapunov exponents and quasinormal modes. *Phys. Rev. D*, 79:064016, 2009. [arXiv:0812.1806](#), [doi:10.1103/PhysRevD.79.064016](#). I
- [13] Vitor Cardoso, João L. Costa, Kyriakos Destounis, Peter Hintz, and Aron Jansen. Quasinormal modes and Strong Cosmic Censorship. *Phys. Rev. Lett.*, 120(3):031103, 2018. [arXiv:1711.10502](#), [doi:10.1103/PhysRevLett.120.031103](#). I
- [14] Qingyu Gan, Guangzhou Guo, Peng Wang, and Houwen Wu. Strong cosmic censorship for a scalar field in a Born-Infeld–de Sitter black hole. *Phys. Rev. D*, 100(12):124009, 2019. [arXiv:1907.04466](#), [doi:10.1103/PhysRevD.100.124009](#).
- [15] Qingyu Gan, Peng Wang, Houwen Wu, and Haitang Yang. Strong Cosmic Censorship for a Scalar Field in an Einstein-Maxwell-Gauss-Bonnet-de Sitter Black Hole. *Chin. Phys. C*, 45(2):025103, 2021. [arXiv:1911.10996](#), [doi:10.1088/1674-1137/abccaf](#). I

- [16] E. Berti and K. D. Kokkotas. Quasinormal modes of Reissner-Nordström-anti-de Sitter black holes: Scalar, electromagnetic and gravitational perturbations. *Phys. Rev. D*, 67:064020, 2003. [arXiv:gr-qc/0301052](#), [doi:10.1103/PhysRevD.67.064020](#). I
- [17] Emanuele Berti, Vitor Cardoso, and Andrei O. Starinets. Quasinormal modes of black holes and black branes. *Class. Quant. Grav.*, 26:163001, 2009. [arXiv:0905.2975](#), [doi:10.1088/0264-9381/26/16/163001](#).
- [18] R. A. Konoplya and A. Zhidenko. Quasinormal modes of black holes: From astrophysics to string theory. *Rev. Mod. Phys.*, 83:793–836, 2011. [arXiv:1102.4014](#), [doi:10.1103/RevModPhys.83.793](#).
- [19] Gregory B. Cook and Maxim Zaluskiy. Purely imaginary quasinormal modes of the Kerr geometry. *Class. Quant. Grav.*, 33(24):245008, 2016. [arXiv:1603.09710](#), [doi:10.1088/0264-9381/33/24/245008](#).
- [20] R. A. Konoplya, A. Zhidenko, and A. F. Zinhailo. Higher order WKB formula for quasinormal modes and grey-body factors: recipes for quick and accurate calculations. *Class. Quant. Grav.*, 36:155002, 2019. [arXiv:1904.10333](#), [doi:10.1088/1361-6382/ab2e25](#). I
- [21] Richard Brito, Vitor Cardoso, and Paolo Pani. *Superradiance: New Frontiers in Black Hole Physics*, volume 906. Springer, 2015. [arXiv:1501.06570](#), [doi:10.1007/978-3-319-19000-6](#). I
- [22] O. Klein. Die Reflexion von Elektronen an einem Potentialsprung nach der relativistischen Dynamik von Dirac. *Z. Phys.*, 53:157, 1929. [doi:10.1007/BF01339716](#). I
- [23] Vitor Cardoso and Paolo Pani. Tidal acceleration of black holes and superradiance. *Class. Quant. Grav.*, 30:045011, 2013. [arXiv:1205.3184](#), [doi:10.1088/0264-9381/30/4/045011](#). I
- [24] R. Penrose. Gravitational collapse: The role of general relativity. *Riv. Nuovo Cim.*, 1:252–276, 1969. [doi:10.1023/A:1016578408204](#). I
- [25] Laurent Di Menza and Jean-Philippe Nicolas. Superradiance on the Reissner–Nordström metric. *Class. Quant. Grav.*, 32(14):145013, 2015. [arXiv:1411.3988](#), [doi:10.1088/0264-9381/32/14/145013](#). I
- [26] Zhiying Zhu, Shao-Jun Zhang, C. E. Pellicer, Bin Wang, and Elcio Abdalla. Stability of Reissner-Nordström black hole in de Sitter background under charged scalar perturbation. *Phys. Rev. D*, 90(4):044042, 2014. [Addendum: *Phys.Rev.D* 90, 049904 (2014)]. [arXiv:1405.4931](#), [doi:10.1103/PhysRevD.90.044042](#). IIB, III, III
- [27] Carolina L. Benone and Luís C. B. Crispino. Superradiance in static black hole spacetimes. *Phys. Rev. D*, 93(2):024028, 2016. [arXiv:1511.02634](#), [doi:10.1103/PhysRevD.93.024028](#). I
- [28] Rodrigo Vicente, Vitor Cardoso, and Jorge C. Lopes. Penrose process, superradiance, and ergoregion instabilities. *Phys. Rev. D*, 97(8):084032, 2018. [arXiv:1803.08060](#), [doi:10.1103/PhysRevD.97.084032](#). I
- [29] Asimina Arvanitaki, Savvas Dimopoulos, Sergei Dubovsky, Nemanja Kaloper, and John March-Russell. String Axiverse. *Phys. Rev. D*, 81:123530, 2010. [arXiv:0905.4720](#), [doi:10.1103/PhysRevD.81.123530](#). I, IV
- [30] S. W. Hawking and G. F. R. Ellis. *The Large Scale Structure of Space-Time*. Cambridge Monographs

- on Mathematical Physics. Cambridge University Press, 2 2011. doi:[10.1017/CB09780511524646](https://doi.org/10.1017/CB09780511524646). I
- [31] Horng Sheng Chia, Christoffel Doorman, Alexandra Wernersson, Tanja Hinderer, and Samaya Nissanke. Self-Interacting Gravitational Atoms in the Strong-Gravity Regime. 12 2022. arXiv:[2212.11948](https://arxiv.org/abs/2212.11948). I
- [32] Emanuele Berti, Vitor Cardoso, and Jose P. S. Lemos. Quasinormal modes and classical wave propagation in analogue black holes. *Phys. Rev. D*, 70:124006, 2004. arXiv:[gr-qc/0408099](https://arxiv.org/abs/gr-qc/0408099), doi:[10.1103/PhysRevD.70.124006](https://doi.org/10.1103/PhysRevD.70.124006). I
- [33] Vitor Cardoso and Oscar J. C. Dias. Small Kerr-anti-de Sitter black holes are unstable. *Phys. Rev. D*, 70:084011, 2004. arXiv:[hep-th/0405006](https://arxiv.org/abs/hep-th/0405006), doi:[10.1103/PhysRevD.70.084011](https://doi.org/10.1103/PhysRevD.70.084011).
- [34] Vitor Cardoso, Oscar J. C. Dias, Jose P. S. Lemos, and Shijun Yoshida. The Black hole bomb and superradiant instabilities. *Phys. Rev. D*, 70:044039, 2004. [Erratum: *Phys.Rev.D* 70, 049903 (2004)]. arXiv:[hep-th/0404096](https://arxiv.org/abs/hep-th/0404096), doi:[10.1103/PhysRevD.70.049903](https://doi.org/10.1103/PhysRevD.70.049903).
- [35] Oscar J. C. Dias, Takaaki Ishii, Keiju Murata, Jorge E. Santos, and Benson Way. Gregory-Laflamme and Superradiance encounter Black Resonator Strings. 12 2022. arXiv:[2212.01400](https://arxiv.org/abs/2212.01400).
- [36] Zhen Li. Superradiance Instability and Quasinormal Modes of the Gravitational Perturbation around Rotating Hairy Black Hole. 12 2022. arXiv:[2212.08112](https://arxiv.org/abs/2212.08112).
- [37] Hao Yang and Yan-Gang Miao. Superradiance of massive scalar particles around rotating regular black holes. 11 2022. arXiv:[2211.15130](https://arxiv.org/abs/2211.15130). I
- [38] Shahar Hod. Stability of the extremal Reissner-Nordstroem black hole to charged scalar perturbations. *Phys. Lett. B*, 713:505–508, 2012. arXiv:[1304.6474](https://arxiv.org/abs/1304.6474), doi:[10.1016/j.physletb.2012.06.043](https://doi.org/10.1016/j.physletb.2012.06.043). I, II B, III A
- [39] Juan Carlos Degollado and Carlos A. R. Herdeiro. Time evolution of superradiant instabilities for charged black holes in a cavity. *Phys. Rev. D*, 89(6):063005, 2014. arXiv:[1312.4579](https://arxiv.org/abs/1312.4579), doi:[10.1103/PhysRevD.89.063005](https://doi.org/10.1103/PhysRevD.89.063005). I
- [40] Carlos A. R. Herdeiro, Juan Carlos Degollado, and Helgi Freyr Rúnarsson. Rapid growth of superradiant instabilities for charged black holes in a cavity. *Phys. Rev. D*, 88:063003, 2013. arXiv:[1305.5513](https://arxiv.org/abs/1305.5513), doi:[10.1103/PhysRevD.88.063003](https://doi.org/10.1103/PhysRevD.88.063003).
- [41] Sam R Dolan, Supakchai Ponglertsakul, and Elizabeth Winstanley. Stability of black holes in Einstein-charged scalar field theory in a cavity. *Phys. Rev. D*, 92(12):124047, 2015. arXiv:[1507.02156](https://arxiv.org/abs/1507.02156), doi:[10.1103/PhysRevD.92.124047](https://doi.org/10.1103/PhysRevD.92.124047).
- [42] Nicolas Sanchis-Gual, Juan Carlos Degollado, Carlos Herdeiro, Jos   A. Font, and Pedro J. Montero. Dynamical formation of a Reissner-Nordstr  m black hole with scalar hair in a cavity. *Phys. Rev. D*, 94(4):044061, 2016. arXiv:[1607.06304](https://arxiv.org/abs/1607.06304), doi:[10.1103/PhysRevD.94.044061](https://doi.org/10.1103/PhysRevD.94.044061). I
- [43] Theodoros Kolyvaris, Marina Koukouvaou, Antri Machattou, and Eleftherios Papantonopoulos. Superradiant instabilities in scalar-tensor Horndeski theory. *Phys. Rev. D*, 98(2):024045, 2018. arXiv:[1806.11110](https://arxiv.org/abs/1806.11110), doi:[10.1103/PhysRevD.98.024045](https://doi.org/10.1103/PhysRevD.98.024045). I
- [44] Yang Huang and Dao-Jun Liu. Charged scalar perturbations around a regular magnetic black hole. *Phys. Rev. D*, 93(10):104011, 2016. arXiv:[1509.09017](https://arxiv.org/abs/1509.09017), doi:[10.1103/PhysRevD.93.104011](https://doi.org/10.1103/PhysRevD.93.104011). I, II B,

III, III

- [45] Carlos A.R. Herdeiro, Eugen Radu, Nicolas Sanchis-Gual, and José A. Font. Spontaneous Scalarization of Charged Black Holes. *Phys. Rev. Lett.*, 121(10):101102, 2018. [arXiv:1806.05190](#), [doi:10.1103/PhysRevLett.121.101102](#). I, II A
- [46] Pedro G. S. Fernandes, Carlos A. R. Herdeiro, Alexandre M. Pombo, Eugen Radu, and Nicolas Sanchis-Gual. Spontaneous Scalarisation of Charged Black Holes: Coupling Dependence and Dynamical Features. *Class. Quant. Grav.*, 36(13):134002, 2019. [Erratum: *Class.Quant.Grav.* 37, 049501 (2020)]. [arXiv:1902.05079](#), [doi:10.1088/1361-6382/ab23a1](#). I
- [47] Pedro G.S. Fernandes, Carlos A.R. Herdeiro, Alexandre M. Pombo, Eugen Radu, and Nicolas Sanchis-Gual. Charged black holes with axionic-type couplings: Classes of solutions and dynamical scalarization. *Phys. Rev. D*, 100(8):084045, 2019. [arXiv:1908.00037](#), [doi:10.1103/PhysRevD.100.084045](#).
- [48] Jose Luis Blázquez-Salcedo, Carlos A.R. Herdeiro, Jutta Kunz, Alexandre M. Pombo, and Eugen Radu. Einstein-Maxwell-scalar black holes: the hot, the cold and the bald. *Phys. Lett. B*, 806:135493, 2020. [arXiv:2002.00963](#), [doi:10.1016/j.physletb.2020.135493](#). I
- [49] De-Cheng Zou and Yun Soo Myung. Scalarized charged black holes with scalar mass term. *Phys. Rev. D*, 100(12):124055, 2019. [arXiv:1909.11859](#), [doi:10.1103/PhysRevD.100.124055](#). I
- [50] Pedro G.S. Fernandes. Einstein-Maxwell-scalar black holes with massive and self-interacting scalar hair. *Phys. Dark Univ.*, 30:100716, 2020. [arXiv:2003.01045](#), [doi:10.1016/j.dark.2020.100716](#). I
- [51] Yan Peng. Scalarization of horizonless reflecting stars: neutral scalar fields non-minimally coupled to Maxwell fields. *Phys. Lett. B*, 804:135372, 2020. [arXiv:1912.11989](#), [doi:10.1016/j.physletb.2020.135372](#). I
- [52] Yun Soo Myung and De-Cheng Zou. Instability of Reissner–Nordström black hole in Einstein-Maxwell-scalar theory. *Eur. Phys. J. C*, 79(3):273, 2019. [arXiv:1808.02609](#), [doi:10.1140/epjc/s10052-019-6792-6](#). I
- [53] Yun Soo Myung and De-Cheng Zou. Stability of scalarized charged black holes in the Einstein–Maxwell–Scalar theory. *Eur. Phys. J. C*, 79(8):641, 2019. [arXiv:1904.09864](#), [doi:10.1140/epjc/s10052-019-7176-7](#).
- [54] De-Cheng Zou and Yun Soo Myung. Radial perturbations of the scalarized black holes in Einstein-Maxwell-conformally coupled scalar theory. *Phys. Rev. D*, 102(6):064011, 2020. [arXiv:2005.06677](#), [doi:10.1103/PhysRevD.102.064011](#).
- [55] Yun Soo Myung and De-Cheng Zou. Onset of rotating scalarized black holes in Einstein-Chern-Simons-Scalar theory. *Phys. Lett. B*, 814:136081, 2021. [arXiv:2012.02375](#), [doi:10.1016/j.physletb.2021.136081](#).
- [56] Zhan-Feng Mai and Run-Qiu Yang. Stability analysis of a charged black hole with a nonlinear complex scalar field. *Phys. Rev. D*, 104(4):044008, 2021. [arXiv:2101.00026](#), [doi:10.1103/PhysRevD.104.044008](#). I
- [57] Dumitru Astefanesei, Carlos Herdeiro, João Oliveira, and Eugen Radu. Higher dimensional black hole

- scalarization. *JHEP*, 09:186, 2020. [arXiv:2007.04153](#), [doi:10.1007/JHEP09\(2020\)186](#). I
- [58] Yun Soo Myung and De-Cheng Zou. Quasinormal modes of scalarized black holes in the Einstein–Maxwell–Scalar theory. *Phys. Lett. B*, 790:400–407, 2019. [arXiv:1812.03604](#), [doi:10.1016/j.physletb.2019.01.046](#). I
- [59] Jose Luis Blázquez-Salcedo, Carlos A.R. Herdeiro, Sarah Kahlen, Jutta Kunz, Alexandre M. Pombo, and Eugen Radu. Quasinormal modes of hot, cold and bald Einstein-Maxwell-scalar black holes. 8 2020. [arXiv:2008.11744](#). I
- [60] Yun Soo Myung and De-Cheng Zou. Scalarized charged black holes in the Einstein-Maxwell-Scalar theory with two U(1) fields. *Phys. Lett. B*, 811:135905, 2020. [arXiv:2009.05193](#), [doi:10.1016/j.physletb.2020.135905](#). I
- [61] Yun Soo Myung and De-Cheng Zou. Scalarized black holes in the Einstein-Maxwell-scalar theory with a quasitopological term. *Phys. Rev. D*, 103(2):024010, 2021. [arXiv:2011.09665](#), [doi:10.1103/PhysRevD.103.024010](#). I
- [62] Hong Guo, Xiao-Mei Kuang, Eleftherios Papantonopoulos, and Bin Wang. Topology and spacetime structure influences on black hole scalarization. 12 2020. [arXiv:2012.11844](#). I
- [63] Yves Brihaye, Betti Hartmann, Nathália Pio Aprile, and Jon Urrestilla. Scalarization of asymptotically anti-de Sitter black holes with applications to holographic phase transitions. *Phys. Rev. D*, 101(12):124016, 2020. [arXiv:1911.01950](#), [doi:10.1103/PhysRevD.101.124016](#). I
- [64] Yves Brihaye, Carlos Herdeiro, and Eugen Radu. Black Hole Spontaneous Scalarisation with a Positive Cosmological Constant. *Phys. Lett. B*, 802:135269, 2020. [arXiv:1910.05286](#), [doi:10.1016/j.physletb.2020.135269](#).
- [65] Cheng-Yong Zhang, Peng Liu, Yunqi Liu, Chao Niu, and Bin Wang. Dynamical charged black hole spontaneous scalarization in Anti-de Sitter spacetimes. 3 2021. [arXiv:2103.13599](#).
- [66] Guangzhou Guo, Peng Wang, Houwen Wu, and Haitang Yang. Scalarized Einstein–Maxwell-scalar black holes in anti-de Sitter spacetime. *Eur. Phys. J. C*, 81(10):864, 2021. [arXiv:2102.04015](#), [doi:10.1140/epjc/s10052-021-09614-7](#). I
- [67] Qingyu Gan, Peng Wang, Houwen Wu, and Haitang Yang. Photon spheres and spherical accretion image of a hairy black hole. *Phys. Rev. D*, 104(2):024003, 2021. [arXiv:2104.08703](#), [doi:10.1103/PhysRevD.104.024003](#). I
- [68] Qingyu Gan, Peng Wang, Houwen Wu, and Haitang Yang. Photon ring and observational appearance of a hairy black hole. *Phys. Rev. D*, 104(4):044049, 2021. [arXiv:2105.11770](#), [doi:10.1103/PhysRevD.104.044049](#). I
- [69] Guangzhou Guo, Xin Jiang, Peng Wang, and Houwen Wu. Gravitational Lensing by Black Holes with Multiple Photon Spheres. 4 2022. [arXiv:2204.13948](#). I
- [70] Yiqian Chen, Guangzhou Guo, Peng Wang, Houwen Wu, and Haitang Yang. Appearance of an infalling star in black holes with multiple photon spheres. *Sci. China Phys. Mech. Astron.*, 65(12):120412, 2022. [arXiv:2206.13705](#), [doi:10.1007/s11433-022-1986-x](#). I

- [71] Hai-Shan Liu, Zhan-Feng Mai, Yue-Zhou Li, and H. Lü. Quasi-topological Electromagnetism: Dark Energy, Dyonic Black Holes, Stable Photon Spheres and Hidden Electromagnetic Duality. *Sci. China Phys. Mech. Astron.*, 63:240411, 2020. [arXiv:1907.10876](#), [doi:10.1007/s11433-019-1446-1](#). I
- [72] Claudia de Rham, Gregory Gabadadze, and Andrew J. Tolley. Resummation of Massive Gravity. *Phys. Rev. Lett.*, 106:231101, 2011. [arXiv:1011.1232](#), [doi:10.1103/PhysRevLett.106.231101](#).
- [73] Ruifeng Dong and Dejan Stojkovic. Gravitational wave echoes from black holes in massive gravity. *Phys. Rev. D*, 103(2):024058, 2021. [arXiv:2011.04032](#), [doi:10.1103/PhysRevD.103.024058](#). I
- [74] Guangzhou Guo, Yuhang Lu, Peng Wang, Houwen Wu, and Haitang Yang. Black Holes with Multiple Photon Spheres. 12 2022. [arXiv:2212.12901](#). I
- [75] Guangzhou Guo, Peng Wang, Houwen Wu, and Haitang Yang. Quasinormal modes of black holes with multiple photon spheres. *JHEP*, 06:060, 2022. [arXiv:2112.14133](#), [doi:10.1007/JHEP06\(2022\)060](#). I, III B
- [76] Guangzhou Guo, Peng Wang, Houwen Wu, and Haitang Yang. Echoes from hairy black holes. *JHEP*, 06:073, 2022. [arXiv:2204.00982](#), [doi:10.1007/JHEP06\(2022\)073](#). I
- [77] R. A. Konoplya and A. Zhidenko. Massive charged scalar field in the Kerr-Newman background I: quasinormal modes, late-time tails and stability. *Phys. Rev. D*, 88:024054, 2013. [arXiv:1307.1812](#), [doi:10.1103/PhysRevD.88.024054](#). III
- [78] Pedro V. P. Cunha, Carlos Herdeiro, Eugen Radu, and Nicolas Sanchis-Gual. The fate of the light-ring instability. 7 2022. [arXiv:2207.13713](#). IV
- [79] Zhen Zhong, Vitor Cardoso, and Elisa Maggio. On the instability of ultracompact horizonless spacetimes. 11 2022. [arXiv:2211.16526](#). IV